Present and LGM permafrost from climate simulations: contribution of statistical downscaling

G. Levavasseur, M. Vrac, Didier M. Roche, D. Paillard, A. Martin, J. Vandenberghe

The Cryosphere Discuss., 4, 2233–2275, 2010
www.the-cryosphere-discuss.net/4/2233/2010/
doi:10.5194/tcd-4-2233-2010

The Cryosphere Discussions

Present and LGM permafrost from climate simulations: contribution of statistical downscaling

G. Levavasseur[1], M. Vrac[1], D. M. Roche[1,2], D. Paillard[1], A. Martin[1], and J. Vandenberghe[2]

[1]Laboratoire des Sciences du Climat et de L'Environnement (LSCE), UMR 8212, IPSL – CEA/CNRS-INSU/UVSQ, Centre d'étude de Saclay, Orme des Merisiers, 91191 Gif-sur-Yvette, France
[2]Section Climate Change and Landscape Dynamics, Department of Earth Sciences, Faculty of Earth and Life Sciences, VU University Amsterdam, de Boelelaan 1085, 1081 HV Amsterdam, The Netherlands

Received: 10 September 2010 – Accepted: 8 October 2010 – Published: 25 October 2010

Correspondence to: G. Levavasseur (guillaume.levavasseur@lsce.ipsl.fr)

Published by Copernicus Publications on behalf of the European Geosciences Union.

Abstract

We quantify the agreement between permafrost distributions from PMIP2 (Paleoclimate Modeling Intercomparison Project) climate models and permafrost data. We evaluate the ability of several climate models to represent permafrost and assess the inter-variability between them.

Studying an heterogeneous variable such as permafrost implies to conduct analysis at a smaller spatial scale compared with climate models resolution. Our approach consists in applying statistical downscaling methods (SDMs) on large- or regional-scale atmospheric variables provided by climate models, leading to local permafrost modelling. Among the SDMs, we first choose a transfer function approach based on Generalized Additive Models (GAMs) to produce high-resolution climatology of surface air temperature (SAT). Then, we define permafrost distribution over Eurasia by SAT conditions. In a first validation step on present climate (CTRL period), GAM shows some limitations with non-systemic improvements in comparison with the large-scale fields. So, we develop an alternative method of statistical downscaling based on a stochastic generator approach through a Multinomial Logistic Regression (MLR), which directly models the probabilities of local permafrost indices. The obtained permafrost distributions appear in a better agreement with data. In both cases, the provided local information reduces the inter-variability between climate models. Nevertheless, this also proves that a simple relationship between permafrost and the SAT only is not always sufficient to represent local permafrost.

Finally, we apply each method on a very different climate, the Last Glacial Maximum (LGM) time period, in order to quantify the ability of climate models to represent LGM permafrost. Our SDMs do not significantly improve permafrost distribution and do not reduce the inter-variability between climate models, at this period. We show that LGM permafrost distribution from climate models strongly depends on large-scale SAT. The differences with LGM data, larger than in the CTRL period, reduce the contribution of downscaling and depend on several factors deserving further studies.

TCD

4, 2233–2275, 2010

1 Introduction

Permafrost reacts to climate change (Harris et al., 2009) with critical feedbacks (Khvorostyanov et al., 2008; Tarnocai et al., 2009), especially on carbon storage and greenhouse gases emissions (Zimov et al., 2006; Beer, 2008). This issue becomes an important subject of interest for future in Arctic regions (Stendel and Christensen, 2002; Lawrence and Slater, 2005; Zhang et al., 2008). Through these feedback processes, the permafrost plays a significant role in climate and in climate models response to global change. Three main approaches exist to model permafrost:

i. some land-models simulate permafrost properties (Nicolsky et al., 2007; Koven et al., 2009) only from climate data; but the permafrost representation depends on the resolution of climate models which cannot reflect the local physical processes involved.

ii. a dynamical model of permafrost can be forced by climate conditions and computes the complex permafrost physics and dynamics as the interactions with snow cover or hydrological network (Delisle, 1998). This method is mainly used to study mountain permafrost (Guglielmin et al., 2003) or to focus on a small region (Marchenko et al., 2008) because it needs large computing time and local data about soil properties (vegetation, lithology, geology, etc.).

iii. the permafrost index can be derived from climatic variables using simple conditions as in Anisimov and Nelson (1997) or Renssen and Vandenberghe (2003).

For simplicity, we start with the hypothesis from Renssen and Vandenberghe (2003) that permafrost depends solely on surface air temperature (SAT, hereafter referred to as "temperature") and presented in Sect. 2 with the used permafrost databases. Applying these temperature conditions, we are able to extract a permafrost index from climate models outputs. In this article, we will assign the name of "climate model (CM)" indifferently to GCMs (Global Circulation Models) or EMICs (Earth Models of Intermediate

TCD
4, 2233–2275, 2010

Complexity). These CMs need a lot of computing time. In order to be able to simulate long time periods, the equations of atmospheric or oceanic dynamics are resolved on coarse spatial grids. Coarse scales cannot reflect the atmospheric local evolutions. Permafrost is an heterogeneous variable related to local climate. Hence, downscaling methods, bringing local information, are useful to compare local permafrost data with global or regional results from climate models. Moreover, coarse resolutions generate a strong variability from one model to another: for example, with the state-of-the-art climate models, the predictions of mean temperature change for the next century range from 1.4 to 3.8 °C for B2 scenario (Meehl et al., 2007). Downscaling could also reduce the inter-variability between CMs, especially at CTRL period. Indeed downscaling defines a model to reproduce calibration data. Hence, different CTRL simulations associated with different downscaling models will both be close to calibration data reducing the differences between several downscaled CMs.

Downscaling is the action of generating climate variables or characteristics at the local scale as a "smart numerical zoom" applied to CMs. On one hand, Regional Climate Models (RCMs) represent the physical approach. They have a higher spatial resolution than CMs and can compute some sub-scale atmospheric processes, parameterized in CMs. RCMs are often used in permafrost studies. Stendel et al. (2007) combine a RCM driven by global climate outputs with a dynamical model of permafrost to bridge the gap between GCMs and local permafrost data. Christensen and Kuhry (2000) derive permafrost from RCM simulation using the "frost index" described originally by Nelson and Outcalt (1987). However, Salzmann et al. (2007) emphasize the need to use different RCMs to reduce uncertainties and to perform sensitivity studies. Nevertheless RCMs are computationally very expensive. On the other hand, the statistical downscaling methods (SDMs) are less resource-intensive and represent an alternative to quickly obtain high-resolution fields from several different CMs. Such an approach consists in using statistical relationships between large-scale variables and the local-scale variable of interest. For instance in permafrost context, Anisimov et al. (2002) use a stochastic model to map the thickness of the soil layer with annual freezing and

TCD
4, 2233–2275, 2010

thawing (the "active-layer"). Among the many existing SDMs, like "weather generators" (Wilby et al., 1998; Wilks, 1999) or "weather typing" (Zorita and von Storch, 1999; Vrac and Naveau, 2007) methods, we choose in Sect. 3 to directly model these relationships by transfer functions (Huth, 2002; Vrac et al., 2007a). To obtain a local permafrost index, we apply the conditions from Renssen and Vandenberghe (2003) on downscaled temperatures using a Generalized Additive Model (GAM – Vrac et al., 2007a; Martin et al., 2010a), allowing to quantify the agreement between simulated high-resolution permafrost and local permafrost data. GAM is suitable for continuous variable as surface temperature but compels to fix the relationship between temperature and permafrost (a discrete variable). So, we develop in Sect. 4 an alternative SDM based on a Multinomial Logistic Regression (MLR) which models directly the relationship between local permafrost and global-scale variables. In climatology, the logistic regression is often employed to model wet or dry day sequences (Buishand et al., 2003; Vrac et al., 2007b; Fealy and Sweeney, 2007) or vegetation types distribution (Calef et al., 2005). In our case, MLR produces a relationship between the probabilities of occurrence of each permafrost category and several continuous variables. For both approaches, a strong hypothesis is to consider the climate as a steady-state and to assume that the permafrost is in equilibrium with it.

Otherwise, climate modelling needs to determine the ability of CMs in simulating past climates in comparison with data. In paleoclimatology, discrepancies appear between CMs and data-proxies intimately related to their close paleo-environments (Gladstone et al., 2005; Ramstein et al., 2007; Otto-Bliesner et al., 2009). Downscaling may reduce these differences between climate models and data. Furthermore, an important exercise is to evaluate the ability of the two statistical models to represent the permafrost distribution of a very different climate. An application of these methods to the Last Glacial Maximum (LGM) is discussed in Sect. 5. We choose to work with a representative set of CMs from the Paleoclimate Modeling Intercomparison Project (PMIP2) (Braconnot et al., 2007a,b) which provides climate simulations for the preindustrial (CTRL, hereafter refered to as "present") and LGM time periods.

TCD
4, 2233–2275, 2010

We summarize our conclusions in Sect. 6.

2 Permafrost: definition and data

Permafrost is defined as ground permanently at or below the freezing point of water for two or more consecutive years (French, 2007). To validate our statistical models on present climate we use geological observations from several authors reviewed and grouped into one circum-artic permafrost map by the International Permafrost Association (IPA) and the Frozen Ground Data Center (FGDC) (Heginbottom et al., 1993; Brown et al., 1997). Most of permafrost data are observations between 1960 and 1980. LGM data correspond to a recent map of permafrost extent maximum in Europe and Asia around 21 ky BP, based on geological observations as described in Vandenberghe et al. (2008) and (2010). Consequently, our region of interest corresponds to the Eurasian continent with the Greenland ice-sheet approximately from 65° E to 175° W and from 20° N to 85° N (see Fig. 1). We consider the Greenland ice-sheet in order to calibrate our statistical model with the widest possible present temperature range for a downscaling on the LGM climate. These two maps have been drawn in a similar way and both datasets describe the spatial distribution of two main types of permafrost (French, 2007):

- continuous permafrost is a permanently frozen ground which covers more than 80% of the sub-soil.
- discontinuous permafrost covers between 30% and 80% of sub-soil. The permanently frozen ground forms in sheltered spots, with possible pockets of unfrozen ground.

TCD
4, 2233–2275, 2010

3 Downscaling with a Generalized Additive Model (GAM)

A GAM cannot directly simulate a discrete variable such as permafrost. We thus decide to downscale the temperatures from different CMs with the same approach as Vrac et al. (2007b) and Martin et al. (2010a). Then, we deduce permafrost from the local temperatures using a simple relationship between permafrost and temperature. This methodology is illustrated in Fig. 2 (left half).

3.1 Temperature data and permafrost relationship

To calibrate our GAM, we need observations. The local-scale data used for the downscaling scheme are the gridded temperature climatology from the Climate Research Unit (CRU) database (New et al., 2002). For each grid-point the dataset counts twelve monthly means from 1961 to 1990 at a regular spatial resolution of $10'$ (i.e. 1/6 degree in longitude and latitude) corresponding to our downscaling resolution. Although this period corresponds to the permafrost observations, permafrost is probably not in equilibrium with present climate and more with preindustrial simulations from CMs. In the following, we will consider the climate as the steady-state and assume that the permafrost is in equilibrium with it.

In order to obtain the permafrost limits from the downscaled temperatures, we derive a local permafrost index according to the hypothesis that permafrost depends solely on temperature. Several relationships exist in literature (Nechaev, 1981; Huijzer and Isarin, 1997), we use the following conditions from Renssen and Vandenberghe (2003) (explicitly described in Vandenberghe et al., 2004), which we will assign the name "RV":

- continuous permafrost:
  annual mean temperature $\leqslant -8\,^{\circ}\mathrm{C}$ and
  coldest month mean temperature $\leqslant -20\,^{\circ}\mathrm{C}$.
- discontinuous permafrost:
  annual mean temperature $\leqslant -4\,^{\circ}\mathrm{C}$.

TCD
4, 2233–2275, 2010

To check the consistency of this assumption of permafrost being only related to temperature, Fig. 1 compares the permafrost distribution obtained by applying these temperature conditions on CRU climatology, with the permafrost index from IPA/FGDC. The similarities between both representations are obvious and show a consistent relationship between the two variables. Some differences exist in high mountains regions on the type or presence of permafrost. Indeed, even if this isotherm combination is calibrated on the present climate, the temperature is not the only criteria to model permafrost: for example, snow cover, soil and vegetation types have key roles for mountain permafrost (Guglielmin et al., 2003; French, 2007). Nevertheless to a first order, deriving permafrost from temperature is a reasonable approximation for present-day conditions.

3.2 Generalized Additive Model

We first use a statistical model applied by Vrac et al. (2007a) to downscale climatological variables and based on the Generalized Additive Models (GAMs) as precisely studied in this context by Martin et al. (2010a). GAM models statistical relationships between local-scale observations (called predictand) and large-scale variables (called predictors), generally from fields of CMs. The large-scale predictors will be described in Sect. 3.2.1. More precisely, this kind of statistical model models the expectation of the explained variable Y (the predictand, surface temperature in our case) by a sum of nonlinear regressions with cubic splines (f_k), conditionally on the predictors X_k (Hastie and Tibshirani, 1990):

$$E(Y_i|X_{k,k=1\ldots n}) = \sum_{k=1}^{n} f_k(X_{i,k}) + \epsilon, \quad (1)$$

where ϵ is the residual or error, n is the number of predictors and i is the grid-cell.

To use GAM, we need to precise the distribution family of the explained variable. For simplicity, we assume that temperature have a gaussian distribution which implies

TCD
4, 2233–2275, 2010

a zero-mean gaussian error ϵ (Hastie and Tibshirani, 1990). Then, any SDM needs a calibration/projection procedure. The calibration is the fitting process of the splines on present climate. Afterward, we project on a different climate to compute a temperature climatology in each grid-point of our region. Initially, the calibration step takes into account the 12 months of the climatology (annual calibration). To be evaluated in fair conditions, the statistical model requires independent data between the calibration and projection steps. Using climatology data does not satisfy this condition on present climate with an annual calibration. As a workaround, we adapt a "cross-validation" procedure which consists in a calibration on 11 months and a projection on the remaining month. With a rotation of this month, we are able to project a local-scale climatology for any month.

In this paper, we only use GAM as a "tool" and we do not directly discuss the behavior of the statistical model; for more details we refer the reader to Vrac et al. (2007a); Martin et al. (2010a,b) and to the "mgcv" R package reference manual (downloadable at http://cran.r-project.org/).

3.2.1 Explanatory variables (predictors)

Previous studies from Vrac et al. (2007a) and Martin et al. (2010a) lead us to select four informative predictors for temperature downscaling, fully described in their studies. Note that we only downscale on the continents because CRU data are only defined on land grid-points. Most of the predictors are computed from a representative set of coupled ocean-atmosphere simulations provided by the Paleoclimate Modeling Intercomparison Project (PMIP2) using state-of-the-art CMs. We choose to work with nine of them listed in Table 1. The explanatory variables may be divided into two groups: the "physical" predictors and the "geographical" ones. The "physical" predictors are directly extracted from CMs outputs and depend on climate dynamics. The "geographical" predictors provide information to our large- vs. local-scale relationships that is robust and stable with time.

TCD
4, 2233–2275, 2010

Here only one "physical" predictor is used and corresponds to the surface air temperature (SAT). This variable is extracted from present and LGM simulations from CMs bilinearly interpolated at 10′ resolution. If the interpolation may have an impact on our downscaling, we do not discuss this point in this study. A first test (not shown) reveals a cold bias from the nine CMs. Indeed, the present (preindustrial) simulations from PMIP2 do not correspond to the 1961–1990 period of CRU data particularly in terms of CO_2 concentration. To account for this effect and to have a more relevant calibration we correct CMs temperatures by adding for each CM the mean difference between itself and CRU climatology before calibration. For LGM period, we do not assume any temporal shift of the simulations. Consequently, we do not apply a similar correction on LGM temperatures and we consider LGM permafrost in equilibrium with LGM climate.

The "geographical" predictors are the topography and two continentality indices. The surface elevation from CMs depends on the resolution and does not account for small orographic structures. To take into account the effect of local topography, we use the high-resolution gridded dataset, ETOPO2[1], from the National Geophysical Data Center (NGDC) which gathers several topographic and bathymetric sources from satellite data and relief models (Amante and Eakins, 2008). We build the LGM topography from ETOPO2 adding in each grid-point a value corresponding to the difference between LGM and present orography. This difference is calculated using the ice-sheet model GRISLI (Peyaud et al., 2007) to account for the ice-sheet elevation and subsidence, and the sea-level changes. The first continentality index is the "diffusive" continentality (DCO). DCO is between 0 and 100% and can be assimilated to the shortest distance to the ocean, 0 being at the ocean edge and 100 being very remote from any ocean. The physical interpretation is the effect of coastal atmospheric circulation on temperature. DCO does not depend on time and is only affected by sea-level change (or land-sea distribution). The second continentality index is the "advective" continentality (ACO).

[1]Computerized digital images and associated databases are available from the National Geophysical Data Center, National Oceanic and Atmospheric Administration, US Department of Commerce, http://www.ngdc.noaa.gov/.

TCD
4, 2233–2275, 2010

ACO is somewhat similar to DCO albeit being modulated by the large-scale wind intensities and directions from CMs and represents an index of the continentalization of air masses. It is based on the hypothesis that an air parcel becomes progressively continental as it travels over land. Hence ACO depends on the changes of land-sea distribution and on wind fields coming from the CMs simulations.

3.2.2 GAM results on present climate

In this section, GAM is applied to the nine CMs from the PMIP2 database. In order to make a visual comparison with data and to highlight the influence of downscaling on permafrost modelling, we compare permafrost distributions deduced from interpolated and from downscaled temperatures for each CM. We will assign the name of "GAM-RV" for the procedure which consists in applying the RV conditions on temperatures downscaled by GAM. In the following, we only discuss the results from two representative models: on the one side ECHAM5 ("ECHAM") is heavily influenced by downscaling and shows the best results on CTRL period. One the other side, IPSL-CM4 ("IPSL") is the coldest CM leading to good downscaling results on LGM. Note that we also mask the ice-sheets (Greenland and Fennoscandia for LGM) as the presence of permafrost under an ice-sheet is not obvious and is currently debated. For example, Cutler et al. (2000) showed that a subglacial permafrost occurred during LGM with a numerical flow-line model. Harris and Murton (2005) argued, on the contrary, that variable degrees of interaction exist between permafrost and glacial phenomena depending on proximity to ice masses, exchanges of energy and transfers of water and ice. They concluded that the presence of ice-cover fundamentally alters the geothermal regime within a permafrost region. Moreover, since our estimate is based on surface temperature there is no reason why the permafrost under the ice-sheet shall be mainly driven by surface temperature, above the ice-sheet.

TCD
4, 2233–2275, 2010

Figures 3a and 4a compare permafrost extents from interpolated temperatures (respectively for ECHAM and IPSL) when applying the RV conditions to derive permafrost, with the permafrost distribution from IPA/FGDC. The two maps reveal a lot of differences between CMs and data at high latitudes and in mountain regions, especially in Himalayas for ECHAM and in eastern Siberia for IPSL. Even if IPSL has a higher resolution (Table 1), improving the representation of regional topographic structures, it does not contain enough local information to represent the permafrost distribution from IPA/FGDC data. Applying our GAM-RV approach, we obtain the corresponding Figs. 3b and 4b. Downscaling shows better permafrost distributions, particularly for discontinuous permafrost at high latitudes. For both CMs, some differences with data disappear and the major contribution of local topography clearly appears for ECHAM with the onset of colder temperatures over the Siberian mounts or Himalayas. However, the information provided by inferred local temperatures cannot reduce the differences on the Scandinavian peninsula and around Himalayas or in eastern Siberia for IPSL.

To quantitatively assess the effect of our downscaling on permafrost representation, we measure the agreement between CMs and data for CTRL period with different numerical indices whose results are listed in Table 2. The first necessary informations are the total permafrost area (PA) and the permafrost area difference with data (PD). Without GAM-RV downscaling, CMs underestimate the permafrost area. Contrary to our expectations, the PA and consequently the PD decrease with GAM-RV downscaling of about 10^6 km^2 for both CMs in comparison with interpolated fields. In order to distinguish between continuous and discontinuous permafrost, we detail their respective areas (CPA and DPA). The decrease of permafrost area is mainly explained by a decrease of the continuous permafrost area of about 0.8×10^6 km^2 for both CMs. The DPA slightly increases for ECHAM ($+0.2 \times 10^6$ km^2) and decreases (-0.3×10^6 km^2) for IPSL. To quantify the proportion of permafrost simulated in right location, %CP (%DP) is the percentage of continuous (discontinuous) permafrost in agreement with data and corresponds to the ratio of blue (turquoise) area on Figs. 3 and 4 over the continuous (discontinuous) area from data. If GAM-RV decreases %CP of about 5% in both

TCD
4, 2233–2275, 2010

cases, it increases %DP from 16 to 31% for ECHAM, while it decreases for IPSL. The responses of these two climate models show the limits of the GAM method. On average GAM-RV essentially enhances the discontinuous permafrost distribution (+4%DP), more reducing the continuous permafrost area (-0.9×10^6 km^2) than increasing the discontinuous permafrost extent ($+0.1 \times 10^6$ km^2). Moreover, Fig. 5a shows the box-and-whisker plots for all interpolated and downscaled CMs. We confirm the decrease of permafrost area for most of downscaled CMs by GAM-RV with a mean relative difference with data of −25.2% against −20.4% for the interpolated CMs. The plots also reveal a weaker inter-variability between CMs with downscaling. Indeed, in Table 2 our GAM-RV reduces the standard deviation for all area indices (for example, from 0.7 to 0.5 for PA).

These area indices provide numerical information on the permafrost extents but do not quantify the statistical relevance of agreement between CMs and data. To judge if we do not obtain these results "by chance", we use the kappa coefficient (κ). This index between 0 and 1 measures the intensity or quality of the agreement based on a simple counting of grid-points in a confusion/matching matrix (Cohen, 1960; Fleiss et al., 1969). The following example details the calculation of the κ coefficient (Eq. 4):

		Model C	Model D	Model N	Total
Data	C	$n_{1,1}$	$n_{1,2}$	$n_{1,3}$	$n_{1,.}$
	D	$n_{2,1}$	$n_{2,2}$	$n_{2,3}$	$n_{2,.}$
	N	$n_{3,1}$	$n_{3,2}$	$n_{3,3}$	$n_{3,.}$
Total		$n_{.,1}$	$n_{.,2}$	$n_{.,3}$	n

$$P_{\text{obs}} = \frac{1}{n}\sum_{i=1}^{3} n_{i,i}, \tag{2}$$

TCD
4, 2233–2275, 2010

$$P_{\text{chance}} = \frac{1}{n^2} \sum_{i=1}^{3} n_{i,.} \times n_{.,i}, \quad (3)$$

$$\kappa = \frac{P_{\text{obs}} - P_{\text{chance}}}{1 - P_{\text{chance}}}, \quad (4)$$

where "C", "D" and "N" corresponds to our three categories "Continuous", "Discontinuous" and "No" permafrost, $n_{i,j}$ are the cell counts with the classification totals $n_{i.}$ and $n_{.j}$, n is the number of grid-cells, P_{obs} (Eq. 2) is the proportion of observed agreement and P_{chance} (Eq. 3) is the proportion of random agreement or expected by chance with independent samples.

Without downscaling, ECHAM obtains a κ of 0.64 and 0.68 for IPSL. To gauge the strength of agreement without an arbitrary scale, we use the kappa maximum ($\kappa_{\max}$). Based on the same counting as the κ, it estimates the best possible agreement (the maximum attainable κ). We adjust the cell counts ($n_{i,j}$) maximizing the agreement (cells $n_{i,j=i}$) keeping the same classification totals of each category for CMs and data ($n_{i.}$ and $n_{.j}$): this allows a more appropriate scaling of κ (Sim and Wright, 2005). The difference between κ and 1 indicates the total unachieved agreement. Accordingly, the difference between κ and $\kappa_{\max}$ indicates the unachieved agreement beyond chance and the difference between $\kappa_{\max}$ and 1 shows the effect on agreement of pre-existing factors that tend to produce unequal classification totals, such as nonlinearities or different sensitivities of CMs. Moreover to provide useful information to interpret the magnitude of κ coefficient, we add the percentage of $\kappa_{\max}$ reached by κ ($\%\kappa_{\max}$). Thus, without downscaling ECHAM (IPSL) reaches 72% (74%) of a maximum agreement beyond chance of 0.88 (0.91). With GAM-RV, the $\%\kappa_{\max}$ increases for both CMs due to an increase of κ and a lower $\kappa_{\max}$. Calculation of the κ coefficient implies intrinsic biases (Cicchetti and Feinstein, 1990). The adjusted kappa (κ_{adj}, also called the prevalence-adjusted bias-adjusted kappa – PABAK) is also based on the same counting as the κ with adjusted cell counts minimizing those intrinsic biases. It gives an indication of the likely effects of biases alongside the true value of κ: if the value of

TCD
4, 2233–2275, 2010

κ_{adj} is close to κ, then the bias is weak (Sim and Wright, 2005). κ_{adj} is necessary to interpret in an appropriate manner the statistical significance of κ coefficient. Here, all studied CMs obtain a κ_{adj} close to their κ. Consequently, the results obtained by GAM-RV are statistically relevant, in better agreement with data and not by chance.

Despite heterogeneous contributions from GAM on permafrost distribution, this method is informative for temperature downscaling on CTRL period. All CMs obtained a percentage of explained variance between 97 and 100%. GAM brings downscaled CMs closer to the CRU climatology improving the temperature distribution (Vrac et al., 2007a; Martin et al., 2010a). We confirm that the RV relationship does not provide enough information for local permafrost distribution and leads to a close dependence between temperature and permafrost. The permafrost distribution from CMs is strongly driven by the latitudinal gradient of SAT, leading to a disagreement with data. Furthermore, applying the RV conditions on CRU temperatures leads to a PA of 10.4×10^6 km^2. Based on the hypothesis that CRU and CTRL permafrost data have no uncertainties, the RV relationship induces an error of −26.0% compared to permafrost data (Fig. 5a). Consequently, GAM-RV includes this error and does not improve the permafrost distribution beyond the CRU permafrost distribution.

4 An alternative approach: the Multinomial Logistic Regression

Using temperature downscaling to reconstruct permafrost limits requires conditions to go from continuous to discrete values. As shown in Sects. 3.1 and 3.2.2, the RV relationship is only based on the contribution of temperature for permafrost distribution. A study at a local-scale needs more informations. Here, we propose to enlarge the spectrum of relationships between permafrost and several factors.

To link a categorical variable, such as permafrost, with several variables, we model the probability of occurrence of permafrost. This probability can take continuous values between 0 and 1. The logistic regression computes the occurrence probability of an event (e.g. permafrost or no permafrost) by fitting data to a logistic function. For

TCD
4, 2233–2275, 2010

instance, Calef et al. (2005) build a hierarchical logistic regression model (three binary logistic regression steps) to predict the potential equilibrium distribution of four major vegetation types. More classically, Fealy and Sweeney (2007) use the logistic regression as SDM to estimate the probabilities of wet and dry days occurrences. Here, we use the logistic regression in its multinomial form (Multinomial Logistic Regression – MLR – Hilbe, 2009; Hosmer and Lemeshow, 2000) to simulate the occurrence probability of a permafrost index, as illustrated in Fig. 2 (right half). MLR is used as a SDM to estimate the occurrence probabilities of the explained variable (Y, permafrost in our case) for each category or class j, taking into account numerical or categorical predictors (X_k):

$$\log\left(\frac{P(Y_i = j)}{1 - P(Y_i = j)}\right) = \sum_{k=1}^{n} \beta_k X_{i,k}, \quad (5)$$

where $P(Y_i = j)$ is the probability of the j-th permafrost category with $\sum_{j=1}^{m} P(Y_i = j) = 1$ (considering m caterogies), β_k are the regression coefficients for the j-th permafrost category, n is the number of predictors and i is the grid-cell.

The method is based on the use of a Generalized Linear Model (GLM – McCullagh and Nelder, 1989). GLM generalizes linear regression using a link function between predictand and predictors unifying various statistical regression models, including linear regression, Poisson regression and logistic regression. For more details see Yee and Wild (1996) and the "VGAM" R package reference manual (downloadable at http://cran.r-project.org/).

Local-scale data used for the calibration step are directly the local-scale observed permafrost indices (IPA/FGDC). In order to compare MLR and GAM-RV we use the same predictors for both methods. As said in Sect. 3.1, the topography, SAT and continentality indices were chosen for temperature downscaling. Although SAT and the topography are clearly necessary for permafrost representation, a study on the predictors choice for permafrost downscaling could be an interesting prospect but is not the purpose of this article.

TCD
4, 2233–2275, 2010

In GAM-RV we had to set the relationship between permafrost and downscaled temperatures. Here, MLR builds a new relationship between permafrost and the selected predictors which can be compared to the previous isotherms combinations from Renssen and Vandenberghe (2003). Figure 6 shows the probabilities to obtain each category of permafrost in each approach. On the panels 6a–c, we apply the RV conditions on CRU temperatures. On the panels 6d–f, we model by MLR the relationship between permafrost from IPA/FGDC and two predictors: the annual mean temperature and the coldest month mean temperature from CRU. Thus, each graph on the left is directly comparable to the corresponding one on the right (Fig. 6). Conditions from Renssen and Vandenberghe (2003) clearly appears with probabilities of 0 or 1 depending on the isotherms described in Sect. 3.1. With MLR, visible similarities with the relationships used in GAM-RV demonstrates the consistency of the method. However, the probabilities can take continuous values between 0 and 1 and allows us to obtain for each grid-point three complementary probabilities for the continuous, discontinuous and no permafrost categories. For example, contrary to GAM-RV, continuous permafrost with a probability of 1 requires a annual mean temperature below −8 °C, but extends to coldest month mean temperatures above −20 °C. In MLR, the modeled relationship also varies according to the selected predictors and the studied CM. Bypassing temperature downscaling allows computing a more complex relationship between predictors and permafrost. Moreover, MLR could take into account other permafrost categories (e.g. sporadic or isolated permafrost; French, 2007).

4.1 Comparison GAM vs. MLR on present climate

To confront MLR with GAM, Figs. 3c and 4c compare the permafrost indices downscaled by MLR (respectively for ECHAM and IPSL) with the permafrost distribution from IPA/FGDC data. The permafrost indices downscaled by MLR correspond in each grid-point to the highest occurrence probability. Permafrost distribution obtained with MLR shows better agreement with data than that obtained with GAM-RV. The contribution of local-scale topography directly improves the discontinuous permafrost representation

TCD
4, 2233–2275, 2010

in Himalayas and Tibetan plateau and in other areas with mountain permafrost (Scandinavian mounts, Alps, Siberian mounts). For both CMs, most of the differences persisting with the GAM downscaling disappear with MLR, as in eastern Siberia for IPSL.

In Table 2, the MLR downscaling improves the permafrost area for ECHAM ($+2.7 \times 10^6$ km^2) and IPSL ($+1.2 \times 10^6$ km^2), increasing the CPA and the DPA in both cases, in comparison with interpolated CMs. The percentages of continuous or discontinuous areas in agreement with data also increase to values close to 90% for %CP and 53% for %DP. The box-and-whisker plot for MLR downscaling (Fig. 5a) clearly shows improvements for all CMs with a mean relative difference with data of −10.6%, compared with GAM-RV (−25.2%).

Moreover, the permafrost distribution is very similar between ECHAM and IPSL. The same patterns can also be observed on the maps of the different CMs (not shown) especially for continuous permafrost. Figure 5a clearly shows that MLR reduces the inter-variability between CMs, more than with GAM-RV. Indeed, MLR has a weaker standard deviation whatever the index (for example, 0.2×10^6 km^2 for PA). This alternative method brings all climate models closer to the permafrost distribution from IPA/FGDC data.

In terms of κ statistics, MLR systematically improves the statistical agreement from 0.64 to 0.79 for ECHAM and from 0.68 to 0.78 for IPSL. No significant changes appears for the κ_{max}. So, the higher $\%\kappa_{max}$ directly reflects a better agreement with data. Note that the standard deviation is also reduced for κ indices: the quality of the agreement is equal for all CMs. MLR provides more confidence on the fact that our results are not obtained "by chance". Moreover, all CMs have a κ_{adj} closer to κ than with GAM-RV: the intrinsic biases are slightly weaker with MLR.

Nevertheless, this method also reveals some inconsistencies. Incorrect transitions from continuous permafrost to no permafrost appear for IPSL (Fig. 4c). A high disagreement on the permafrost category persists at high latitudes for ECHAM (Fig. 3c). As previously mentioned, this is due to the physics included in our statistical model: the predictors choice is relevant for temperature downscaling. Soil temperature, vegetation

TCD
4, 2233–2275, 2010

type and snow cover could bring more consistent physics to build a high-resolution permafrost.

In conclusion, bypassing temperature downscaling provides an adapted relationship between permafrost and predictors for each CM, leading to a more precise spatial representation of permafrost and a better agreement with observed data, at CTRL period.

Our results are the byproduct of several factors such as: the ability of CMs to correctly represent temperature, the relationship between permafrost and chosen variables, etc. It is thus difficult to independently quantify the error of each factor in the final result. Such a sensitivity analysis is beyond the scope of our paper and will be the subject of further studies.

5 Application to LGM permafrost

In a climate change context it is interesting to test the ability of our statistical models to represent past climates when they have been calibrated on present climate. In terms of temperatures and precipitation Martin et al. (2010b) obtain remarkable results from the EMIC CLIMBER (Ganopolski et al., 2001; Petoukhov et al., 2000) in comparison with GCMs outputs for the Last Glacial Maximum (LGM) climate and conclude to a great potential of GAM for applications in paleoclimatology (Vrac et al., 2007a; Martin et al., 2010b).

Can we thus export our statistical models at a different past climate, as the LGM, in terms of permafrost distribution? To answer this question, we apply our two SDMs on LGM outputs from the PMIP2 CMs. For this time period, the permafrost distribution used to compare with CMs is from Vandenberghe et al. (2010).

Figures 7a and 8a compare the permafrost distribution from interpolated CMs (with the RV conditions) with the permafrost distribution from data. Without downscaling, ECHAM and IPSL already appear too warm to correctly represent permafrost limits from data. For ECHAM, the permafrost limits do not comply with the Fennoscandian

TCD
4, 2233–2275, 2010

ice-sheet contours. Moreover, its coarse orography is not enough to represent mountain permafrost in Himalayas. IPSL is colder and has a higher resolution, providing a more representative permafrost distribution around the ice-sheet and the Tibetan plateau. Figures 7b and 8b compare in the same way the permafrost distribution from GAM-RV with the permafrost distribution from Vandenberghe et al. (2010). The contribution of the local-scale topography appears particularly with the onset of mountain permafrost in Himalayas for ECHAM as for present climate. For IPSL, GAM slightly warms temperatures, leading to permafrost limits at higher latitudes. Permafrost downscaled with MLR is compared with data in Figs. 7c and 8c. For the ECHAM model, the local-scale topography also brings up the Himalayas and Tibetan plateau, but the transitions from continuous to no permafrost are more numerous (blue to pink colors on Fig. 7c). MLR applied to IPSL shows a weaker effect of the local topography but the permafrost limits reach lower latitudes than interpolated CMs or GAM-RV, especially the southern regions of the Fennoscandian ice-sheet.

We give in Table 3 the numerical indices for LGM period. Quantitatively, GAM-RV does not systematically improve the permafrost area: +1.4 for ECHAM and -1.6×10^6 km^2 for IPSL with respect to interpolated fields. Even if GAM-RV degrades the permafrost distribution for IPSL, it remains the best representation with the highest %CP (63%) and %DP (7%) for this method. With MLR downscaling, the results are improved for both CMs at the same order than CTRL period (about $+1.5 \times 10^6$ km^2 between interpolated and downscaled CMs). Moreover, we obtain higher %CP and %DP than GAM-RV for all CMs. Nevertheless, with both SDMs the surface differences with data are more important than CTRL period. The CMs underestimates the continuous permafrost area and no or less discontinuous permafrost is simulated in right location (%DP ranges between 0 and 20%). No significant decrease appears in terms of inter-variability between all CMs: the measured standard deviation (Table 3) is higher than CTRL period and remains fairly stable around 3×10^6 km^2 for both SDMs. The box-and-whisker plots in Fig. 5b for LGM clearly show that GAM-RV or MLR faces difficulties to improve the nine climate models. Applying a Fisher's test, the variances from MLR

TCD
4, 2233–2275, 2010

and GAM-RV simulations are not significantly different; same results appears for their means with a Student's test. This shows that the permafrost distribution at the LGM is strongly driven by the large-scale temperature from CMs. Our SDMs cannot correct the large gap between interpolated CMs and permafrost data at LGM (Fig. 5b). With a simulated LGM climate closer to data, downscaling could have more impact: it is the case of the IPSL model with a contribution of downscaling in the same order that CTRL period (Tables 2 and 3). Consequently, we cannot base our interpretation of the LGM results on CTRL results.

The larger differences with data than at CTRL period imply a lower κ coefficient (Table 3). With GAM-RV no changes appear for ECHAM except for the κ_{adj} showing larger biases in calculation of κ. For IPSL the κ coefficient decreases from 0.63 to 0.58. GAM-RV does not improve the statistical agreement, reflecting the weak potential of CMs to correctly represent permafrost limits for the LGM period. MLR obtains the best results improving slightly the agreement with data for all CMs.

We can summarize with some remarks:

i. the contribution of GAM is not sufficient to reduce the gap between CMs and data in reproducing local-scale permafrost. MLR produces a more realistic permafrost distribution reaching latitudes similar to those from data and improving the agreement with it. Nevertheless, our SDMs do not reduce the inter-variability between CMs at LGM.

ii. our SDMs includes the strong contribution of surface temperature and topography. Nevertheless as for CTRL period, the predictors ACO and DCO are not informative for permafrost. So common differences appear between the two periods. Despite consistent patterns, the permafrost distribution is still strongly driven by the latitudinal gradient of SAT for GAM-RV and incorrect transitions from continuous to no permafrost appears with MLR.

iii. with the hypothesis that LGM and CTRL permafrost data have no uncertainties, that the simulated climates from CMs are at equilibrium with permafrost data and

TCD
4, 2233–2275, 2010

that the relationships between permafrost and chosen variables are stable with time, the nine climate models from PMIP2 cannot simulate a cold enough climate to represent the LGM period. They have a warm bias that cannot be completely corrected by one of the two tested SDMs calibrated on present climate.

iv. the differences observed between downscaled CMs and data partly come from the relationship between permafrost and the other variables. The RV conditions are based on present observations. The relationship between permafrost and predictors from MLR is also calibrated on the CTRL period. Do these relationships be the same during the LGM period? The continuous or discontinuous permafrost extents may not be defined by the same isotherms seen in Sect. 3.1; in the case of MLR, the influence of different predictors may change in another climate.

v. finally, LGM permafrost data are best currently available and based on geological observations of the maximum permafrost extent and correspond to the coldest time period around LGM (21 kyr BP). The LGM time period is defined with the maximum extent of the ice-sheets which is probably not directly related to temperature minimum. In the high-resolution record from the North Greenland Ice Core Project (NGRIP, Andersen et al., 2004), the last temperature minimum appears at about 34 kyr BP. A lag may exist between the LGM data and the LGM climate simulated by climate models. Therefore, LGM permafrost data are likely to be overestimated. The differences between downscaled permafrost from PMIP2 models and LGM permafrost extent from Vandenberghe et al. (2010) should be taken as a gross estimate.

6 Conclusions

We described two statistical downscaling methods (SDMs) for permafrost studies. In order to obtain high-resolution permafrost spatial distribution, we first applied these SDMs on climate models outputs for the present climate (CTRL). The approach by

TCD
4, 2233–2275, 2010

Generalized Additive Model (GAM) is suitable for representing the temperature behavior at a local-scale (Vrac et al., 2007b). According to Martin et al. (2010a) results, choosing a GAM leads to a relevant physical model for the small scales with simple statistical relationships that are easily interpretable. Applying the conditions defined by Renssen and Vandenberghe (2003) on downscaled temperatures improves the spatial distribution of discontinuous permafrost but underestimates the permafrost area. This GAM-RV method reaches some limits with a permafrost strongly driven by the latitudinal gradient of temperatures. Indeed a simple combination of isotherms is not sufficient to describe the permafrost distribution at a local-scale. The approach by Multinomial Logistic Regression (MLR) is more adapted for this application. The modeled relationship, as a function of several variables, provides a better representation of continuous permafrost and mountain permafrost (especially discontinuous permafrost) and reduces the inter-variability between all climate models from PMIP2 database with a larger statistical relevance. The results from MLR confirm that a study at a local-scale needs more physics about permafrost.

Applying our SDMs on a different climate, the Last Glacial Maximum (LGM), leads to permafrost distribution in better agreement with data, especially for MLR downscaling. Nevertheless downscaling of LGM permafrost extent faces difficulties with larger differences than CTRL period. None of the studied climate models can represent a LGM permafrost extent comparable to data, whatever the method used. The inter-variability between climate models strongly depends on large-scale temperature that cannot be completely corrected by our SDMs. The differences with data reduce the contribution of downscaling and have different sources: (i) an assumed stationarity of the RV conditions for GAM and the modeled relationship for MLR; (ii) an initial bias from climate models which cannot simulate a proper LGM climate; (iii) a complex permafrost dynamics under-represented in our SDMs by predictors; (iv) a possible lag between the LGM period from climate models and the period represented by data from Vandenberghe et al. (2010). Our approach is thus essentially limited by the ability of climate models to produce correct climatic signal, especially for climates different from CTRL.

TCD
4, 2233–2275, 2010

To complement this study, some points would deserve to be deepened to improve our results. Permafrost is an heterogeneous variable with few observations. Climate models temperature, used to derive permafrost distribution, is a global and continuous variable. Therefore, we need local-scale predictors that will add local variability to climate signal. Our SDMs use local-scale topography but other variables used in permafrost dynamic models, as vegetation or soil properties (Marchenko et al., 2008), are required to have a representative physics of permafrost processes and a better distribution. The potential of the MLR approach lies in the control of the physics included in the predictors. In this study we used the same predictors for both SDMs. It is obvious that they can and should be changed in the MLR method to represent more accurately the permafrost distribution. This ongoing work will take into account large-scale fields of snow cover and thickness and soil temperature. We can also imagine to build new "geographical" predictors such as exposure to the sun depending on the orientation of the topography slope (Brown, 1969). The balancing and choice of "geographical" and "physical" predictors is crucial to maintain good local representation and a consistent and robust physical model applicable to different climates. To reconcile models and data, it would also be interesting to downscale permafrost at colder periods simulated by climate models, such as Heinrich events (Kageyama et al., 2005). We would be able to determine the needed temperatures to obtain the best permafrost limits according to the data from Vandenberghe et al. (2010).

Acknowledgements. We thank J. Vandenberghe (Centre for Geo-ecological Research, Netherlands) for providing permafrost data for the Last Glacial Maximum period, C. Dumas for deriving LGM topography from GRISLI data. G. Levavasseur is supported by UVSQ, D. Roche by INSU/CNRS.

TCD
4, 2233–2275, 2010

The publication of this article is financed by CNRS-INSU.

References

Amante, C. and Eakins, B.: ETOPO1 – 1 arc-minute global relief model: procedures, data sources and analysis, National Geophysical Data Center, NESDIS, NOAA, US Department of Commerce, Boulder, CO, 2008. 2242

Andersen, K., Azuma, N., Barnola, J.-M., Bigler, M., Biscaye, P., Caillon, N., Chappellaz, J., Clausen, B., Dahl-Jensen, D., Fischer, H., Flückiger, J., Fritzsche, D., Fujii, Y., Goto-Azuma, K., Grønvold, K., Gundestrup, N., Hansson, M., Huber, C., Hvidberg, C., Johnsen, S., Jonsell, U., Jouzel, J., Kipfstuhl, S., Landais, A., Leuenberger, M., Lorrain, R., Masson-Delmotte, V., Miller, H., Motoyama, H., Narita, H., Popp, T., Raynaud, D., Rothlisberger, R., Ruth, U., Samyn, D., Schwander, J., Shoji, H., Siggard-Andersen, M.-L., Steffensen, J., Stocker, T., Sveinbjörnsdóttir, A., Svensson, A., Takata, M., Tison, J.-L., Thorsteinsson, T., Watanabe, O., Wilhelms, F., and White, J.: High-resolution record of Northern Hemisphere climate extending into the last interglacial period, Nature, 431, 147–151, doi:10.1038/nature02805, 2004. 2254

Anisimov, O. and Nelson, F.: Permafrost zonation and climate change in the northern hemisphere: results from transient general circulation models, Climatic Change, 35, 241–258, doi:10.1023/A:1005315409698, 1997. 2235

Anisimov, O., Shiklomanov, N., and Nelson, F.: Variability of seasonal thaw depth in permafrost regions: a stochastic modeling approach, Ecol. Model., 153, 217–227, doi:10.1016/S0304-3800(02)00016-9, 2002. 2236

Beer, C.: The arctic carbon count, Nat. Geosci., 1, 569–570, doi:10.1038/ngeo292, 2008. 2235

Braconnot, P., Otto-Bliesner, B., Harrison, S., Joussaume, S., Peterchmitt, J.-Y., Abe-Ouchi, A., Crucifix, M., Driesschaert, E., Fichefet, Th., Hewitt, C. D., Kageyama, M., Kitoh, A., Laîné, A.,

TCD
4, 2233–2275, 2010

Loutre, M.-F., Marti, O., Merkel, U., Ramstein, G., Valdes, P., Weber, S. L., Yu, Y., and Zhao, Y.: Results of PMIP2 coupled simulations of the Mid-Holocene and Last Glacial Maximum - Part 1: experiments and large-scale features, Clim. Past, 3, 261–277, doi:10.5194/cp-3-261-2007, 2007a. 2237

Braconnot, P., Otto-Bliesner, B., Harrison, S., Joussaume, S., Peterchmitt, J.-Y., Abe-Ouchi, A., Crucifix, M., Driesschaert, E., Fichefet, Th., Hewitt, C. D., Kageyama, M., Kitoh, A., Loutre, M.-F., Marti, O., Merkel, U., Ramstein, G., Valdes, P., Weber, L., Yu, Y., and Zhao, Y.: Results of PMIP2 coupled simulations of the Mid-Holocene and Last Glacial Maximum – Part 2: feedbacks with emphasis on the location of the ITCZ and mid- and high latitudes heat budget, Clim. Past, 3, 279–296, doi:10.5194/cp-3-279-2007, 2007b. 2237

Brown, J., Ferrians, O., Heginbottom, J., and Melnikov, E.: Circum-Arctic map of permafrost and ground-ice conditions, Washington, DC: US Geological Survey in Cooperation with the Circum-Pacific Council for Energy and Mineral Resources, Circum-Pacific Map Series, CP-45, 1997. 2238

Brown, R.: Factors influencing discontinuous permafrost in Canada, in: The Periglacial Environment, Past and Present, edited by: Péwé, T., INQUA Seventh Congress, McGill-Queen's University Press, Montreal, Canada, 11–53, 1969. 2256

Buishand, T., Shabalova, M., and Brandsma, T.: On the choice of the temporal aggregation level for statistical downscaling of precipitation, J. Climate, 17, 1816–1827, 2003. 2237

Calef, M., McGuire, A., Epstein, H., Rupp, T., and Shugart, H.: Analysis of vegetation distribution in Interior Alaska and sensitivity to climate change using a logistic regression approach, J. Biogeogr., 32, 863–878, 2005. 2237, 2248

Christensen, J. and Kuhry, P.: High-resolution regional climate model validation and permafrost simulation for the East European Russian Arctic, J. Geophys. Res., 105, 29647–29658, doi:10.1029/2000JD900379, 2000. 2236

Cicchetti, D. and Feinstein, A.: High agreement but low kappa – II. Resolving the paradoxes, J. Clin. Epidemiol., 43, 551–558, doi:10.1016/0895-4356(90)90159-M, 1990. 2246

Cohen, J.: A coefficient of agreement for nominal scales, Educational and Psychological Measurement, 20, 37–46, doi:10.1177/001316446002000104, 1960. 2245

Collins, W., Bitz, C., Blackmon, M., Bonan, G., Bretherton, C., Carton, J., Chang, P., Doney, S., Hack, J., Henderson, T., Kiehl, J., Large, W., McKenna, D., Santer, B., and Smith, R.: The community climate system model: CCSM3, B. Am. Meteorol. Soc., 82, 2357–2376, doi:10.1175/JCLI3761.1, 2001. 2265

TCD
4, 2233–2275, 2010

Cutler, P., MacAyeal, D., Mickelson, D., Parizek, B., and Colgan, P.: A numerical investigation of ice-lobe-permafrost interaction around the southern Laurentide ice-sheet, J. Glaciol., 46, 311–325, 2000. 2243

Delisle, G.: Numerical simulation of permafrost growth and decay, J. Quaternary Sci., 13, 325–333, doi:0.1002/(SICI)1099-1417(199807/08)13:4, 1998. 2235

Driesschaert, E., Fichefet, T., Goosse, H., Huybrechts, P., Janssens, I., Mouchet, A., Munhoven, G., Brovkin, V., and Weber, S. L.: Modeling the influence of Greenland ice sheet melting on the Atlantic meridional overturning circulation during the next millennia, Geophys. Res. Lett., 34, L10707, doi:10.1029/2007GL029516, 2007. 2265

Fealy, R. and Sweeney, J.: Statistical downscaling of precipitation for a selection of sites in Ireland employing a generalised linear modelling approach, Int. J. Climatol., 27, 2083–2094, doi:10.1002/joc.1506, 2007. 2237, 2248

Fleiss, J., Cohen, J., and Everitt, B.: Large sample standard errors of kappa and weighted kappa, Psychol. Bull., 72, 323–327, doi:10.1037/h0028106, 1969. 2245

French, H.: The periglacial environment, 3rd Edition, Wiley, 2007. 2238, 2240, 2249

Ganopolski, A., Petoukhov, V., Rahmstorf, S., Brovkin, V., Claussen, M., Eliseev, A., and Kubatzki, C.: CLIMBER-2: a climate system model of intermediate complexity – Part 2: model sensitivity, Clim. Dynam., 17, 735–751, doi:10.1007/s003820000144, 2001. 2251

Gladstone, R., Ross, I., Valdes, P., Abe-Ouchi, A., Braconnot, P., Brewer, S., Kageyama, M., Kitoh, A., Legrande, A., Marti, O., Ohgaito, R., Otto-Bliesner, B., Peltier, W., and Vettoretti, G.: Mid-Holocene NAO: a PMIP2 model intercomparison, Geophys. Res. Lett., 32, L16707, doi:10.1029/2005GL023596, 2005. 2237

Goosse, H., Brovkin, V., Fichefet, T., Haarsma, R., Huybrechts, P., Jongma, J., Mouchet, A., Selten, F., Barriat, P.-Y., Campin, J.-M., Deleersnijder, E., Driesschaert, E., Goezler, H., Janssens, I., Loutre, M.-F., Maqueda, M., Opsteegh, T., Mathieu, P.-P., Munhoven, G., Pettersson, E., Renssen, H., Roche, D. M., Schaeffer, M., Tartinville, B., Timmermann, A., and Weber, S.: Description of the earth system model of intermediate complexity LOVECLIM version 1.2, Geoscientific Model Development, 3, 309–390, doi:10.5194/gmdd-3-309-2010, 2010. 2265

Gordon, C., Cooper, C., Senior, C., Banks, H., Gregory, J., Johns, T., Mitchell, J., and Wood, R.: The simulation of SST, sea ice extents and ocean heat transports in a version of the Hadley Centre coupled model without flux adjustments, Clim. Dynam., 16, 147–168, doi:10.1007/s003820050010, 2000. 2265

TCD

4, 2233–2275, 2010

Guglielmin, M., Aldighieri, B., and Testa, B.: PERMACLIM: a model for the distribution of mountain permafrost, based on climatic observations, Geomorphology, 51, 245–257, doi:10.1016/S0169-555X(02)00221-0, 2003. 2235, 2240

Harris, C. and Murton, J.: Interactions between glaciers and permafrost: an introduction, Geological Society, London, Special Publications, 242, 1–9, doi:10.1144/GSL.SP.2005.242.01.01, 2005. 2243

Harris, C., Arenson, L., Christiansen, H., Etzelmüller, B., Frauenfelder, R., Gruber, S., Haeberli, W., Hauck, C., Hölzle, M., Humlum, O., Isaksen, K., Kääb, A., Kern-Lütschg, M., Lehning, M., Matsuoka, N., Murton, J., Nötzli, J., Phillips, M., Ross, N., Seppälä, M., Springman, S., and Mühll, D.: Permafrost and climate in Europe: monitoring and modelling thermal, geomorphological and geotechnical responses, Earth-Sci. Rev., 92, 117–171, doi:10.1016/j.earscirev.2008.12.002, 2009. 2235

Hastie, T. and Tibshirani, R.: Generalized Additive Models, Chapman and Hall, London, 1990. 2240, 2241

Hasumi, H. and Emori, S.: K-1 coupled GCM (MIROC), Tech. Rep. 1, Center for Climate System Research (CCSR) and University of Tokyo and National Institute for Environmental Studies (NIES) and Frontier Research Center for Global Change (FRCGC), 2004. 2265

Heginbottom, J., Brown, J., Melnikov, E., and Ferrians, O.: Circum-arctic map of permafrost and ground ice conditions, Sixth International Conference proceeding, 2, 1993. 2238

Hilbe, J.: Logistic Regression Models, Chapman and Hall/CRC, 2009. 2248

Hosmer, D. and Lemeshow, S.: Applied logistic regression, 2nd Edition, Wiley, 2000. 2248

Huijzer, A. and Isarin, R.: The reconstruction of past climates using multi-proxy evidence: an example of the Weichselian Pleniglacial in northwest and central Europe, Quaternary Sci. Rev., 16, 513–533, doi:10.1016/S0277-3791(96)00080-7, 1997. 2239

Huth, R.: Statistical downscaling of daily temperature in Central Europe, J. Climate, 15, 1731–1742, doi:10.1175/1520-0442(2002)015, 2002. 2237

Kageyama, M., Combourieu Nebout, N., Sepulchre, P., Peyron, O., Krinner, G., Ramstein, G., and Cazt, J.-P.: The Last Glacial Maximum and Heinrich Event 1 in terms of climate and vegetation around the Alboran Sea: a preliminary model-data comparison, Compte Rendus Geoscience, 337, 983–992, doi:10.1016/j.crte.2005.04.012, 2005. 2256

Khvorostyanov, D., Ciais, P., Krinner, G., Zimov, S., Corradi, Ch., and Guggenberger, G.: Vulnerability of permafrost carbon to global warming – Part 2: sensitivity of permafrost carbon stock to global warming, Tellus, 60B, 265–275, doi:10.1111/j.1600-0889.2007.00336.x,

TCD
4, 2233–2275, 2010

2008. 2235
Koven, C., Friedlingstein, P., Ciais, P., Khvorostyanov, D., Krinner, G., and Tarnocai, C.: On the formation of high-latitude soil carbon stocks: effects of cryoturbation and insulation by organic matter in a land surface model, Geophys. Res. Lett., 36, L21501, doi: 10.1029/2009GL040150, 2009. 2235
Lawrence, D. and Slater, A.: A projection of severe near-surface permafrost degradation during the 21st century, Geophys. Res. Lett., 32, L24401, doi:10.1029/2005GL025080, 2005. 2235
Marchenko, S., Romanovsky, V., and Tipenko, G.: Numerical modeling of spatial permafrost dynamics in Alaska, in: 9th International Conference on Permafrost, vol. 2, 1125–1130, Fairbanks, Alaska, US, 2008. 2235, 2256
Marti, O., Braconnot, P., Bellier, J., Benshila, R., Bony, S., Brockmann, P., Cadulle, P., Caubel, A., Denvil, S., Dufresne, J.-L., Fairhead, L., Filiberti, M.-A., Fichefet, T., Friedlingstein, P., Grandpeix, J.-Y., Hourdin, F., Krinner, G., Lévy, C., Musat, I., and Talandier, C.: The new IPSL climate system model: IPSL-CM4, Note du Pôle de Modélisation, 26, 1–86, 2005. 2265
Martin, A., Vrac, M., Paillard, D., and Dumas, C.: Statistical-dynamical downscaling for an Earth Model of Intermediate Complexity – Part 1: Methodology and calibrations, Clim. Dynam., submitted, 2010a. 2237, 2239, 2240, 2241, 2247, 2255
Martin, A., Vrac, M., Paillard, D., Dumas, C., and Kageyama, M.: Statistical-dynamical downscaling for an Earth Model of Intermediate Complexity – Part 2: Application to past and future climates, Clim. Dynam., submitted, 2010b. 2241, 2251
McCullagh, P. and Nelder, J.: Generalized Linear Models, 2nd Edition, Chapman and Hall/CRC, 1989. 2248
Meehl, G., Stocker, T., Collins, W., Friedlingstein, P., Gaye, A., Gregory, J., Kitoh, A., Knutti, R., Murphy, J., Noda, A., Raper, S., Watterson, I., Weaver, A., and Zhao, Z.-C.: Global Climate Projections, Climate Change 2007: The Physical Science Basis. Contribution of Working Group I to the Fourth Assessment Report of the Intergovernmental Panel on Climate Change, 749–845, 2007. 2236
Nechaev, V.: On some relations between parameters of permafrost and their paleogeographic application, Problems of Pleistocene paleogeography in glacial and periglacial regions, 211–220, 1981. 2239
Nelson, F. and Outcalt, S.: A computational method for prediction and regionalization of permafrost, Artic and Alpine Research, 19, 279–288, 1987. 2236

TCD
4, 2233–2275, 2010

New, M., Lister, D., Hulme, M., and Makin, I.: A high-resolution data set of surface climate over global land areas, Clim. Res., 21, 1–25, doi:10.3354/cr021001, 2002. 2239
Nicolsky, D., Romanovsky, V., Alexeev, V., and Lawrence, D.: Improved modeling of permafrost dynamics in a GCM land-surface scheme, Geophys. Res. Lett., 34, L08501, doi:10.1029/2007GL029525, 2007. 2235
Otto-Bliesner, B., Schneider, R., Brady, E., Kucera, M., Abe-Ouchi, A., Bard, E., Braconnot, P., Crucifix, M., Hewitt, C., Kageyama, M., Marti, O., Paul, A., Rosell-Melé, A., Waelbroeck, C., Weber, S., Weinelt, M., and Yu, Y.: A comparison of PMIP2 model simulations and the MARGO proxy reconstruction for tropical sea surface temperatures at last glacial maximum, Clim. Dynam., 32, 799–815, doi:10.1007/s00382-008-0509-0, 2009. 2237
Petoukhov, V., Ganopolski, A., Brovkin, V., Claussen, M., Eliseev, A., Kubatzki, C., and Rahmstorf, S.: CLIMBER-2: a climate system model of intermediate complexity – Part 1: model description and performance for present climate, Clim. Dynam., 16, 1–17, doi:10.1007/PL00007919, 2000. 2251
Peyaud, V., Ritz, C., and Krinner, G.: Modelling the Early Weichselian Eurasian Ice Sheets: role of ice shelves and influence of ice-dammed lakes, Clim. Past, 3, 375–386, doi:10.5194/cp-3-375-2007, 2007. 2242
Pope, V., Gallani, M., Rowntree, P., and Stratton, R.: The impact of new physical parametrizations in the Hadley Centre climate model: HadAM3, Clim. Dynam., 16, 123–146, doi:10.1007/s003820050009, 2000. 2265
Ramstein, G., Kageyama, M., Guiot, J., Wu, H., Hély, C., Krinner, G., and Brewer, S.: How cold was Europe at the Last Glacial Maximum? A synthesis of the progress achieved since the first PMIP model-data comparison, Clim. Past, 3, 331–339, doi:10.5194/cp-3-331-2007, 2007. 2237
Renssen, H. and Vandenberghe, J.: Investigation of the relationship between permafrost distribution in NW Europe and extensive winter sea-ice cover in the North Atlantic Ocean during the cold phases of the Last Glaciation, Quaternary Sci. Rev., 22, 209–223, doi:10.1016/S0277-3791(02)00190-7, 2003. 2235, 2237, 2239, 2249, 2255, 2273
Roeckner, E., Bauml, G., Bonaventura, L., Brokopf, R., Esch, M., Giorgetta, M., Hagemann, S., Kirchner, I., Kornblueh, L., Manzini, E., Rhodin, A., Schlese, U., Schulzweida, U., and Tompkins, A.: The atmospheric general circulation model ECHAM5 – Part 1: Model description, Tech. rep., Max-Planck-Institute for Meteorology, 2003. 2265
Salas-Mélia, D., Chauvin, F., Déqué, M., Douville, H., Guérémy, J., Marquet, P., Planton, S.,

TCD
4, 2233–2275, 2010

Royer, J., and Tyteca, S.: Description and validation of the CNRM-CM3 global coupled model, CNRM working note 103, 2005. 2265
Salzmann, N., Frei, C., Vidale, P.-L., and Hoelzle, M.: The application of Regional Climate Model output for the simulation of high-mountain permafrost scenarios, Global Planet. Change, 56, 188–202, doi:10.1016/j.gloplacha.2006.07.006, 2007. 2236
Sim, J. and Wright, C.: The kappa statistic in reliability studies: use, interpretation, and sample size requirements, Phys. Ther., 85, 257–268, 2005. 2246, 2247
Stendel, M. and Christensen, J.: Impact of global warming on permafrost conditions in a coupled GCM, Geophys. Res. Lett., 29, 1632, doi:10.1029/2001GL014345, 2002. 2235
Stendel, M., Romanovsky, V., Christensen, J., and Sazonova, T.: Using dynamical downscaling to close the gap between global change scenarios and local permafrost dynamics, Global Planet. Change, 56, 203–214, doi:10.1016/j.gloplacha.2006.07.014, 2007. 2236
Tarnocai, C., Canadell, J., Schuur, E., Kuhry, P., Mazhitova, G., and Zimov, S.: Soil organic carbon pools in the northern circumpolar permafrost region, Global Biogeochem. Cy., 23, GB2023, doi:10.1029/2008GB003327, 2009. 2235
Vandenberghe, J., Lowe, J., Coope, G., Litt, T., and Züller, L.: Climatic and environmental variability in the mid-latitude Europe sector during the last interglacial-glacial cycle, in: Past Climate Variability through Europe and Africa, edited by: Battarbee, R., Gasse, F., and Stickley, C., Springer Netherlands, 6, 393–416, 2004. 2239
Vandenberghe, J., Velichko, A., and Gorbunov, A.: Forcing factors of permafrost retreat: a comparison between LGM and present-day permafrost extent in Eurasia, in: 9th International Conference Permafrost, edited by: Kane, D. and Hinkel, K., 327–328, 2008. 2238
Vandenberghe, J., Renssen, H., Roche, D., Goosse, H., Velichko, A., Gorbunov, A., and Levavasseur, G.: Eurasian permafrost instability constrained by reduced sea-ice cover, in preparation, 2010. 2238, 2251, 2252, 2254, 2255, 2256, 2267, 2272, 2274, 2275
Vrac, M. and Naveau, P.: Stochastic downscaling of precipitation: from dry events to heavy rainfalls, Water Resour. Res., 43, W07402, doi:10.1029/2006WR005308, 2007. 2237
Vrac, M., Marbaix, P., Paillard, D., and Naveau, P.: Non-linear statistical downscaling of present and LGM precipitation and temperatures over Europe, Clim. Past, 3, 669–682, doi:10.5194/cp-3-669-2007, 2007a. 2237, 2240, 2241, 2247, 2251
Vrac, M., Stein, M., and Hayhoe, K.: Statistical downscaling of precipitation through nonhomogeneous stochastic weather typing, Clim. Res., 34, 169–184, doi:10.3354/cr00696, 2007b. 2237, 2239, 2255

TCD
4, 2233–2275, 2010

Wilby, R., Wigley, T., Conway, D., Jones, P., Hewitson, B., Main, J., and Wilks, D.: Statistical downscaling of general circulation model output: A comparison of methods, Water Resour. Res., 34, 2995–3008, doi:10.1029/98WR02577, 1998. 2237

Wilks, D.: Multisite downscaling of daily precipitation with a stochastic weather generator, Clim. Res., 11, 125–136, 1999. 2237

Yee, T. and Wild, C.: Vector Generalized Additive Models, Journal of Royal Statistical Society, 58, 481–493, 1996. 2248

Yongqiang, Y., Rucong, Y., Xuehong, Z., and Hailong, L.: A flexible global coupled climate model, Adv. Atmos. Sci., 19, 169–190, 2002. 2265

Yongqiang, Y., Xuehong, Z., and Yufu, G.: Global coupled ocean-atmosphere general circulation models in LASG/IAP, Adv. Atmos. Sci., 21, 444–455, doi:10.1007/BF02915571, 2004. 2265

Zhang, Y., Chen, W., and Risborough, D.: Transient projections of permafrost distribution in Canada during the 21st century under scenarios of climate change, Global Planet. Change, 60, 443–456, doi:10.1016/j.gloplacha.2007.05.003, 2008. 2235

Zimov, S., Schuur, E., and Chapin, F.: Permafrost and the global permafrost and the global carbon budget, Science, 312, 1612–1613, doi:10.1126/science.1128908, 2006. 2235

Zorita, E. and von Storch, H.: The analog method as a simple statistical downscaling technique: comparison with more complicated methods, J. Climate, 12, 2474–2489, doi:10.1175/1520-0442(1999)012, 1999. 2237

TCD
4, 2233–2275, 2010

Table 1. PMIP2 models references (resolutions are in LON × LAT).

N°	Model	Resolution	Laboratory	References
1	CCSM	128 × 64	National Center of Atmospheric Research (NCAR), USA	Collins et al. (2001)
2	CNRM	128 × 64	Centre National de Recherche Scientifique (CNRM)	Salas-Mélia et al. (2005)
3	LOVECLIM	64 × 32	Université Catholique de Louvain	Driesschaert et al. (2007) Goosse et al. (2010)
4	ECHAM5	96 × 48	Max Planck Institute for Meteorology (MPIM)	Roeckner et al. (2003)
5	FGOALS	128 × 60	State Key Laboratory of Numerical Modeling for Atmospheric Sciences and Geophysical Fluid Dynamics (LASG)	Yongqiang et al. (2002, 2004)
6	HadCM3	96 × 73	Hadley Centre	Gordon et al. (2000) Pope et al. (2000)
7	IPSL-CM4	96 × 72	Institut Pierre Simon Laplace	Marti et al. (2005)
8	MIROC3.2.2	128 × 64	Center for Climate System Research, University of Tokyo	Hasumi and Emori (2004)
9	MIROC3.2	128 × 64	Center for Climate System Research, University of Tokyo	Hasumi and Emori (2004)

TCD
4, 2233–2275, 2010

Table 2. PMIP2 quantitative results for CTRL period. Mean and standard deviation are computed with the nine CMs. "DATA" column corresponds to IPA/FGDC permafrost index. The PA, CPA, DPA and PD indices are respectively set for total permafrost, continuous permafrost, discontinuous permafrost areas and total permafrost difference with data and are expressed in 10^6 km^2. The %CP and %DP indices are respectively the percentages of continuous and discontinuous permafrost in agreement with data. The κ, κ_{max}, κ_{adj} indices corresponds respectively to the κ coefficient, its maximum value and its adjusted value. The $\%\kappa_{max}$ is the percentage of κ_{max} reached by κ. Numbers from 1 to 9 correspond to the PMIP2 models referenced in Fig. 1.

PMIP2 Models		DATA	1	2	3	4	5	6	7	8	9	Mean	Std. dev.
Interpolated	PA	14.1	10.2	10.0	10.0	10.7	11.3	11.2	11.1	12.0	11.9	10.9	0.7
	CPA	6.9	6.5	5.6	6.4	7.4	5.8	6.5	5.9	8.5	8.3	6.8	1.1
	%CP	100	84	66	82	89	69	81	73	90	89	80	9
	DPA	7.2	3.7	4.4	3.7	3.3	5.4	4.7	5.2	3.5	3.6	4.2	0.8
	%DP	100	30	26	27	16	32	32	35	21	22	27	6
	PD	0.0	−4.0	−4.1	−4.1	−3.4	−2.9	−2.9	−3.1	−2.2	−2.2	−3.2	0.7
	κ	–	0.71	0.61	0.69	0.64	0.62	0.68	0.68	0.66	0.66	0.66	0.03
	κ_{max}	–	0.87	0.87	0.86	0.88	0.93	0.92	0.91	0.88	0.89	0.89	0.02
	$\%\kappa_{max}$	–	82	71	80	72	67	74	74	75	75	75	4
	κ_{adj}	–	0.79	0.73	0.78	0.74	0.72	0.77	0.76	0.75	0.75	0.76	0.02
GAM-RV downscaled	PA	14.1	10.3	10.4	9.3	9.8	9.9	10.5	10.0	10.7	10.7	10.2	0.5
	CPA	6.9	6.7	5.2	5.3	6.3	4.3	5.4	5.1	7.3	7.1	5.9	1.0
	%CP	100	82	64	75	84	49	67	67	86	85	73	12
	DPA	7.2	3.6	5.2	3.9	3.5	5.6	5.1	4.9	3.5	3.6	4.3	0.9
	%DP	100	29	33	32	31	30	35	33	27	27	31	3
	PD	0.0	−3.9	−3.7	−4.9	−4.3	−4.3	−3.6	−4.2	−3.4	−3.4	−4.0	0.5
	κ	–	0.71	0.63	0.70	0.72	0.59	0.68	0.67	0.71	0.71	0.68	0.04
	κ_{max}	–	0.86	0.89	0.82	0.84	0.84	0.87	0.86	0.88	0.88	0.86	0.02
	$\%\kappa_{max}$	–	83	72	85	86	70	78	78	80	80	79	5
	κ_{adj}	–	0.80	0.74	0.79	0.80	0.71	0.97	0.77	0.79	0.79	0.77	0.03
MLR downscaled	PA	14.1	12.6	12.3	12.6	12.4	12.2	12.8	12.3	12.6	12.6	12.5	0.2
	CPA	6.9	7.3	7.2	7.3	7.5	7.4	7.5	7.1	7.3	7.3	7.3	0.1
	%CP	100	89	90	89	92	87	90	89	91	91	90	2
	DPA	7.2	5.4	5.1	5.3	5.0	4.8	5.3	5.2	5.2	5.2	5.2	0.2
	%DP	100	55	52	54	54	49	55	52	55	55	53	2
	PD	0.0	−1.5	−1.9	−1.5	−1.7	−2.0	−1.4	−1.9	−1.6	−1.6	−1.7	0.2
	κ	–	0.78	0.77	0.78	0.79	0.75	0.78	0.78	0.79	0.79	0.78	0.01
	κ_{max}	–	0.91	0.90	0.91	0.90	0.88	0.91	0.90	0.91	0.91	0.90	0.01
	$\%\kappa_{max}$	–	86	86	85	89	85	87	86	87	87	86	1
	κ_{adj}	–	0.84	0.83	0.84	0.85	0.82	0.84	0.84	0.85	0.85	0.84	0.01

TCD
4, 2233–2275, 2010

Table 3. PMIP2 quantitative results for LGM period. Mean and standard deviation are computed with the nine CMs. "DATA" column corresponds to Vandenberghe et al. (2010) data. The PA, CPA, DPA and PD indices are respectively set for total permafrost, continuous permafrost, discontinuous permafrost areas and total permafrost difference with data and are expressed in 10^6 km^2. The %CP and %DP indices are respectively the percentages of continuous and discontinuous permafrost in agreement with data. The κ, κ_{max}, κ_{adj} indices corresponds respectively to the κ coefficient, its maximum value and its adjusted value. The $\%\kappa_{max}$ is the percentage of κ_{max} reached by κ. Numbers from 1 to 9 correspond to the PMIP2 models referenced in Fig. 1.

PMIP2 Models		DATA	1	2	3	4	5	6	7	8	9	Mean	Std. dev.
Interpolated	PA	33.8	21.5	17.2	15.7	18.1	17.5	20.4	26.5	19.1	18.2	19.4	3.2
	CPA	29.3	17.0	12.0	10.9	14.1	13.8	15.8	20.2	14.7	13.5	14.7	2.8
	%CP	100	58	41	37	48	47	54	69	50	46	50	9
	DPA	4.5	4.5	5.3	4.8	4.0	3.7	4.6	6.3	4.4	4.6	4.7	0.8
	%DP	100	0	3	1	0	1	0	7	1	1	1	2
	PD	0.0	−12.3	−16.6	−18.1	−15.7	−16.3	−13.4	−7.3	−14.7	−15.6	−14.4	3.2
	κ	–	0.54	0.40	0.39	0.47	0.45	0.50	0.63	0.47	0.44	0.48	0.07
	κ_{max}	–	0.65	0.51	0.49	0.58	0.61	0.62	0.74	0.59	0.55	0.59	0.07
	$\%\kappa_{max}$	–	82	79	78	81	73	82	85	81	80	80	3
	κ_{adj}	–	0.55	0.45	0.29	0.47	0.51	0.43	0.64	0.40	0.36	0.45	0.10
GAM-RV Downscaled	PA	33.8	21.6	17.8	15.3	19.5	17.2	19.6	24.9	18.0	17.1	19.0	2.9
	CPA	29.3	17.4	12.3	9.4	14.5	13.2	14.8	18.4	13.3	12.4	14.0	2.7
	%CP	100	59	42	32	50	45	51	63	45	42	48	9
	DPA	4.5	4.2	5.6	5.9	4.9	4.1	4.8	6.6	4.7	4.7	5.0	0.8
	%DP	100	1	3	1	4	2	0	7	1	1	2	2
	PD	0.0	−12.2	−16.0	−18.5	−14.3	−16.6	−14.2	−8.9	−15.8	−16.7	−14.8	2.9
	κ	–	0.54	0.41	0.35	0.47	0.43	0.48	0.58	0.44	0.41	0.46	0.07
	κ_{max}	–	0.66	0.51	0.45	0.58	0.54	0.59	0.68	0.55	0.52	0.56	0.07
	$\%\kappa_{max}$	–	83	79	77	81	80	81	84	80	79	81	2
	κ_{adj}	–	0.55	0.46	0.24	0.53	0.49	0.40	0.58	0.43	0.40	0.45	0.10
MLR downscaled	PA	33.8	23.0	20.4	18.7	19.9	18.7	21.4	28.4	19.4	18.5	20.9	3.2
	CPA	29.3	17.2	14.6	11.6	15.6	13.3	16.2	19.7	13.5	12.9	14.9	2.5
	%CP	100	59	50	40	53	45	55	67	46	44	51	9
	DPA	4.5	5.8	5.8	7.1	4.3	5.4	5.3	8.7	5.9	5.6	6.0	1.3
	%DP	100	10	11	10	10	9	9	20	9	9	11	4
	PD	0.0	−10.8	−13.4	−15.1	−13.9	−15.1	−12.4	−5.4	−14.4	−15.3	−12.9	3.2
	κ	–	0.55	0.48	0.41	0.50	0.45	0.52	0.64	0.46	0.44	0.49	0.07
	κ_{max}	–	0.66	0.59	0.52	0.66	0.55	0.63	0.73	0.56	0.54	0.60	0.07
	$\%\kappa_{max}$	–	83	82	80	76	81	83	87	81	81	82	3
	κ_{adj}	–	0.56	0.54	0.39	0.51	0.50	0.58	0.64	0.45	0.43	0.51	0.08

TCD
4, 2233–2275, 2010

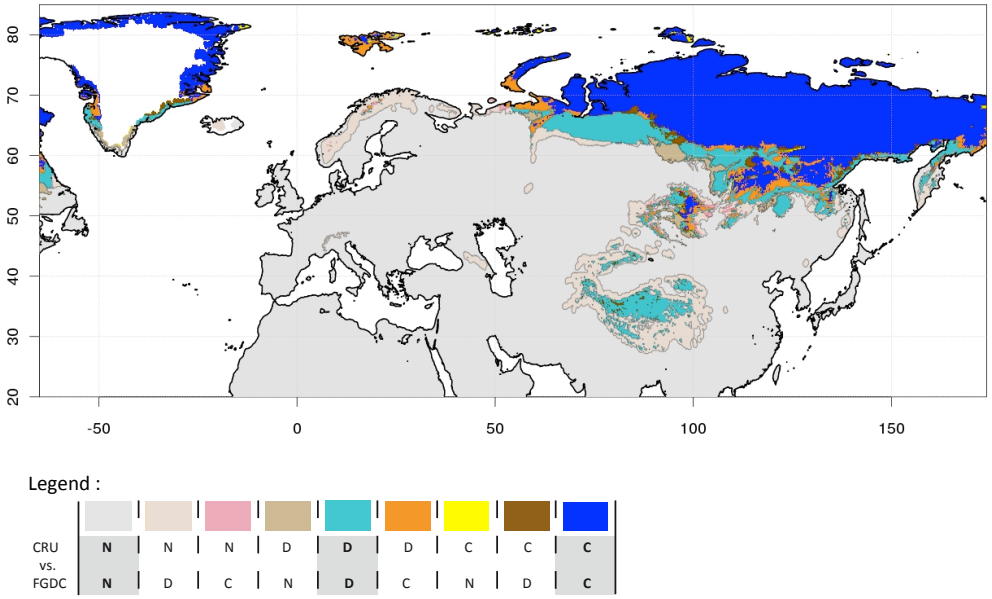

Fig. 1. Permafrost comparison between CRU temperature climatology with the RV conditions and the IPA/FGDC permafrost index. In the legend panel,"N" corresponds to "No permafrost", "D" to "Discontinuous permafrost" and "C" to "Continuous permafrost". The highlighted categories with bold letters shows the agreement between both datasets.

TCD
4, 2233–2275, 2010

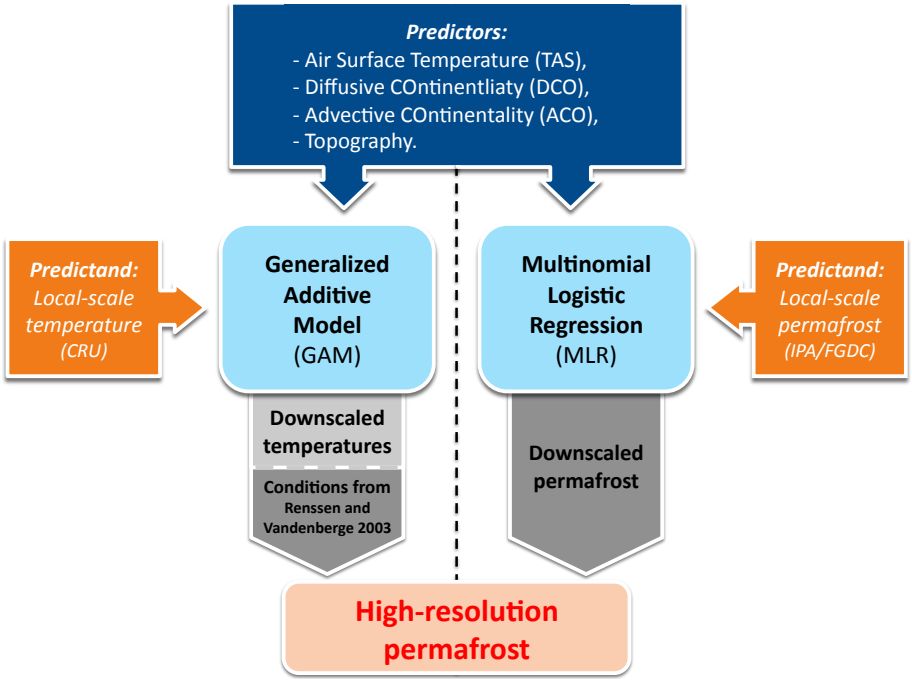

Fig. 2. Schema of the two downscaling procedures.

TCD
4, 2233–2275, 2010

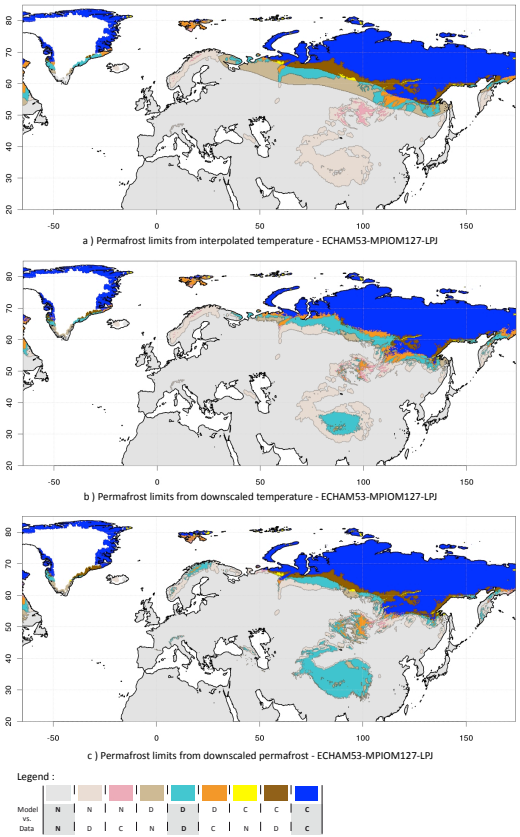

Fig. 3. CTRL permafrost comparison between ECHAM53-MPIOM127-LPJ and the IPA/FGDC permafrost index. **(a)** is obtained with a bilinear interpolation of temperatures and the RV conditions to derive permafrost. **(b)** is the same from the downscaled temperatures by GAM. And **(c)** is the downscaled permafrost index by MLR (c). In the legend panel,"N" corresponds to "No permafrost", "D" to "Discontinuous permafrost" and "C" to "Continuous permafrost". The highlighted categories with bold letters shows the agreement between model and data.

TCD
4, 2233–2275, 2010

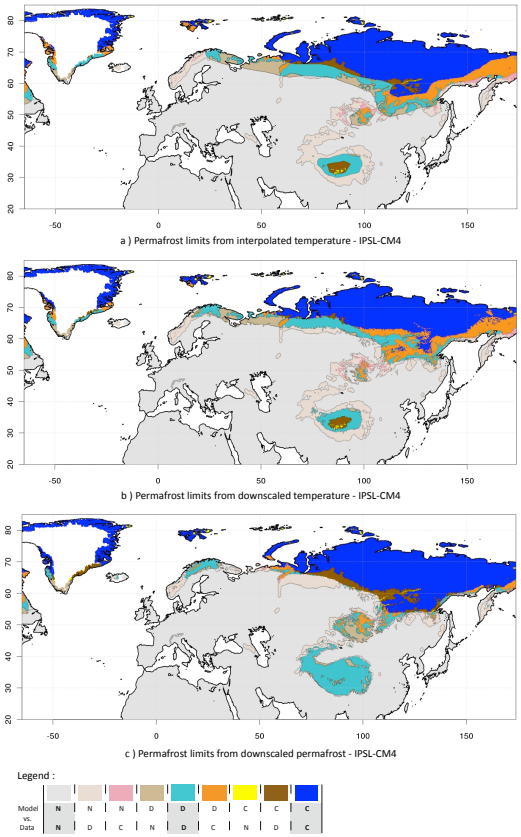

Fig. 4. CTRL permafrost comparison between IPSL-CM4 and the IPA/FGDC permafrost index. **(a)** is obtained with a bilinear interpolation of temperatures and the RV conditions to derive permafrost. **(b)** is the same from the downscaled temperatures by GAM. And **(c)** is the downscaled permafrost index by MLR (c). In the legend panel, "N" corresponds to "No permafrost", "D" to "Discontinuous permafrost" and "C" to "Continuous permafrost". The highlighted categories with bold letters shows the agreement between model and data.

TCD
4, 2233–2275, 2010

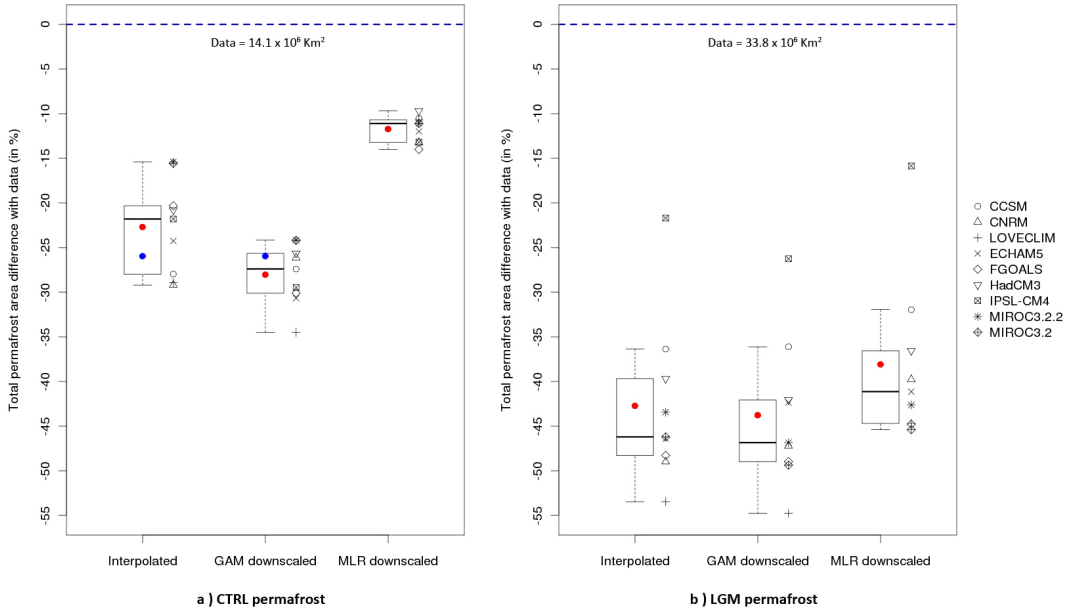

Fig. 5. Total permafrost area relative differences with data for CTRL **(a)** and LGM **(b)** periods. For each period, the relative differences obtained from the interpolated PMIP2 models are on the left; the relative differences from the downscaled CMs by GAM-RV on the middle; and the relative differences from the downscaled CMs by MLR on the right. The values of the nine models are shown by symbols on the right of each box-and-whisker plot, with their means (red bullets). For CTRL period, permafrost relative difference derived from CRU temperatures with the RV relationship is shown with blue bullets. IPA/FGDC (a) and Vandenberghe et al. (2010) (b) data are drawn with blue dashed lines, with their respective values.

TCD
4, 2233–2275, 2010

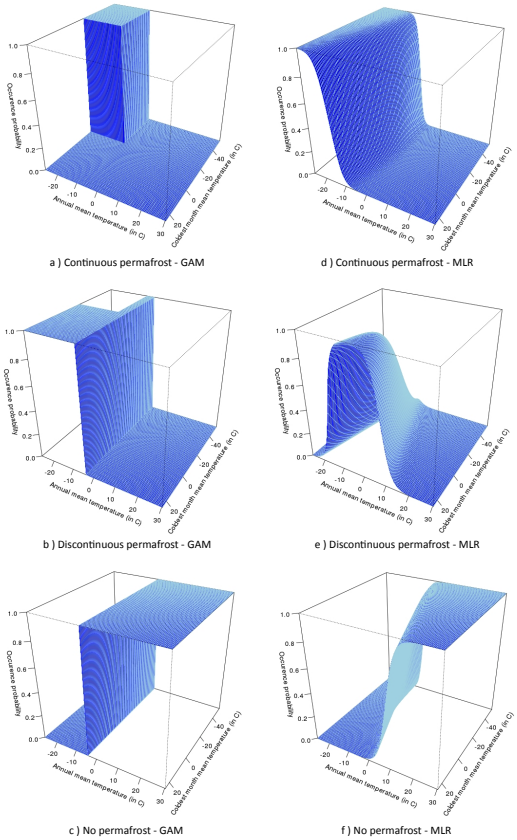

Fig. 6. Permafrost occurrence probabilities based on the annual mean local temperatures and the coldest month mean local temperatures from CRU data. Panels **(a–c)** (on the left) corresponds to the fixed temperature conditions from Renssen and Vandenberghe (2003) (isotherms combinations) used for GAM-RV downscaling method; panels **(d–f)** (on the right) shows the modeled relationship between permafrost and the two same variables by the MLR downscaling method.

TCD
4, 2233–2275, 2010

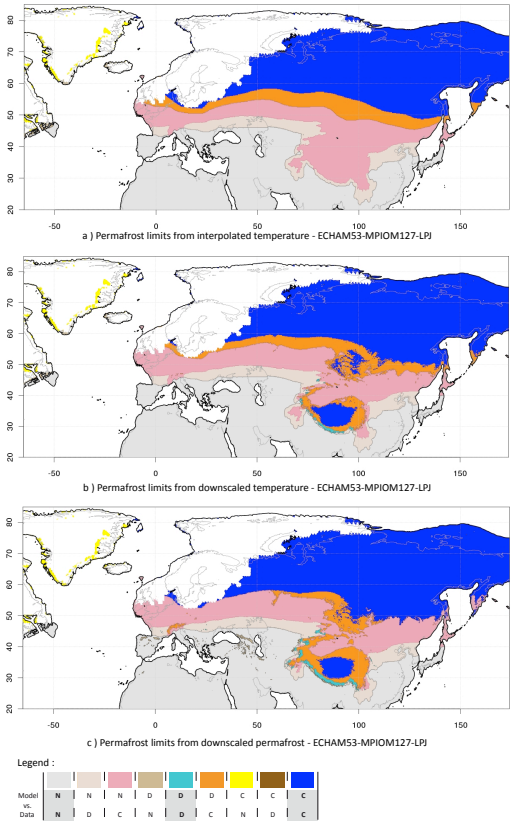

Fig. 7. LGM permafrost comparison between ECHAM53-MPIOM127-LPJ and the Vandenberghe et al. (2010) permafrost index. **(a)** is obtained with a bilinear interpolation of temperatures and the RV conditions to derive permafrost. **(b)** is the same from the downscaled temperatures by GAM. And **(c)** is the downscaled permafrost index by MLR (c). In the legend panel,"N" corresponds to "No permafrost", "D" to "Discontinuous permafrost" and "C" to "Continuous permafrost". The highlighted categories with bold letters shows the agreement between model and data.

TCD
4, 2233–2275, 2010

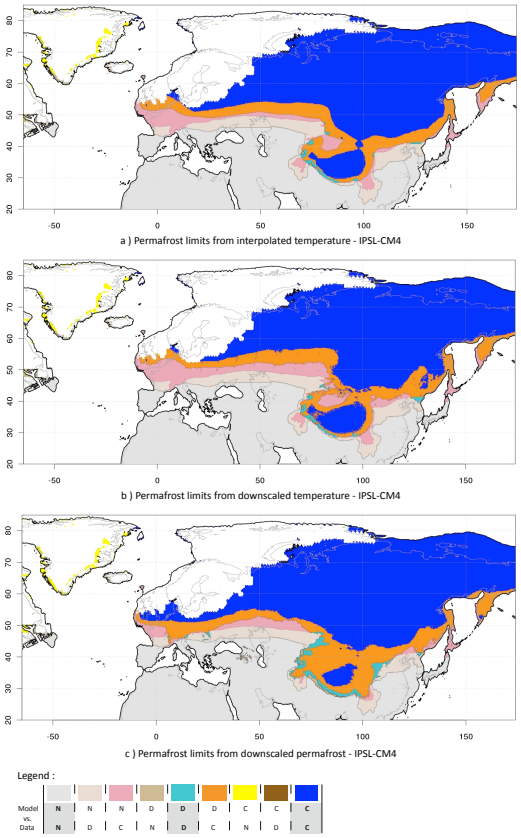

Fig. 8. LGM permafrost comparison between IPSL-CM4 and the Vandenberghe et al. (2010) permafrost index. **(a)** is obtained with a bilinear interpolation of temperatures and the RV conditions to derive permafrost. **(b)** is the same from the downscaled temperatures by GAM. And **(c)** is the downscaled permafrost index by MLR (c). In the legend panel,"N" corresponds to "No permafrost", "D" to "Discontinuous permafrost" and "C" to "Continuous permafrost". The highlighted categories with bold letters shows the agreement between model and data.

TCD
4, 2233–2275, 2010